RSC Advances

PAPER

View Article Online
View Journal | View Issue

Cite this: *RSC Adv.*, 2019, **9**, 24305

Synthesis and luminescence properties of novel $Eu^{2+/3+}$, Ce^{3+} ion single- and co-doped $BaZn_2(PO_4)_2$ phosphors for white-light applications

Yuhan Zhu, Wenjun Wang, Zefeng Xu, Qi Luo, Ling Li* and Xiaoguang Liu*

Received 13th June 2019
Accepted 15th July 2019

DOI: 10.1039/c9ra04442f

rsc.li/rsc-advances

A series of novel $Eu^{2+/3+}$, Ce^{3+} ion single- and co-doped $BaZn_2(PO_4)_2$ samples were prepared *via* a high-temperature solid-state reaction. XRD powder diffraction results indicated that all of the products were pure phases. The photoluminescence properties of $BaZn_2(PO_4)_2$:Eu showed that Eu^{2+} and Eu^{3+} coexist in the system and Eu^{3+} can be self-reduced to Eu^{2+} in an air atmosphere. In addition, the strongest emission peak of Eu^{3+} ions at 593 nm implied that Eu^{3+} ions occupy the inversion symmetry lattice and also the site of Zn in $BaZn_2(PO_4)$. We used the theoretical method of bond energy to explain why the self-reduction of Eu^{3+} to Eu^{2+} can occur in the $BaZn_2(PO_4)_2$ system. The calculation results indicated that the bond energy change value $\Delta E^{Zn}_{Eu^{2+}-O^{2-}}$ is smaller than $\Delta E^{Zn}_{Eu^{3+}-O^{2-}}$, indicating that Eu^{2+} ions are more likely to occupy the Zn site and more stable than Eu^{3+} ions in $BaZn_2(PO_4)$. Furthermore, the energy transfer process between Ce^{3+} and Eu^{2+} ions in the photoluminescence spectrum and the decay lifetime were observed, and the energy transfer mechanism was determined to be a dipole–dipole interaction. In this work, by adjusting the ratio of Ce and Eu ions, the emission color can be changed from blue to white, implying that the phosphor can be used as a promising candidate in the manufacture of white LEDs.

1. Introduction

Rare-earth doped luminescent materials have wide applications in the fields of illumination, display, laser, anti-counterfeiting, fiber-optic communication and biomedicine, and they have become a hotspot in many interdisciplinary research studies. The rare-earth doped white LED materials have drawn extensive attention due to their advantages of luminous efficiency, energy saving, environmental protection, long life, and simple structure.[1–5] Among most rare-earth ions, Eu^{3+} ions have been extensively studied. It is a typical red-emitting rare-earth ion with an electronic structure of $[Xe]4f^6$, and its emission spectrum is caused by an electronic transition from the excited state $^5D_0$ high-energy level to the ^7F_J (J = 0, 1, 2⋯6) ground-state energy level in the 4f configuration. If the Eu^{3+} ion is located at the strict inversion center, its $^5D_0 \rightarrow {}^7F_1$ electronic transition is the strongest at around 590 nm, emitting orange-red light. When the Eu^{3+} ion is deviated from the inversion center position, the $^5D_0 \rightarrow {}^7F_2$ electric dipole transition in the emission spectrum is the strongest at about 612 nm with red light.[6–8] In recent years, the reduction from Eu^{3+} to Eu^{2+} has been found to occur in the same crystal in an air atmosphere. For example, in aluminosilicates[9], aluminate,[10,11] silicate,[12] phosphate,[13] borate,[14,15] the reduction from Eu^{3+} to Eu^{2+} have appeared. The Eu^{2+} spectral position changes with the strength of the crystal field, and ultraviolet, blue, and red light are generated according to the degree of splitting.[16] Ce^{3+} is also an important luminescent ion, and its transition between 4f and 5d is the allowed electric dipole transition; hence, it has high excitation and emission peaks. The interaction of the exposed d-electrons with the crystal field broadens the excitation and emission of Ce^{3+}, and the emission of light can be adjusted from the near-ultraviolet to red region depending on the matrix. This property allows Ce^{3+} ions to spectrally overlap with most common luminescent ions in a specific matrix, greatly increasing the probability and efficiency of energy transfer. When the Ce^{3+} ion is in an excited state, it can transfer energy to the co-doped rare-earth ion by resonance according to the ion spacing, which is a commonly used and excellent sensitizer.[17–19] Ce^{3+} ions can be co-doped with many ions such as Ce^{3+}, Tb^{3+}/Mn^{2+} in $Ca_{19}Ce(PO_4)_{14}$,[20] $CaSc_2O_4:Ce^{3+}$, Yb^{3+},[21] $LiYSiO_4:Ce^{3+}$, Eu^{3+},[22] $BaY_2Si_3O_{10}:Ce^{3+}$, Pr^{3+},[23] $K_2Ba_3Si_8O_{20}:Ce^{3+}$, and Eu^{2+} (ref. 24) to generate energy transfer behavior.

The bond energy theory is used to analyze and explain the priority occupancy for doping ions entering the crystal lattice. The change in bond energy is smaller as per the bond energy theory when the doping ions replace the cation sites in the crystal lattice, in which the easier the doping ions preferentially occupy. At present, this theory has been effectively used in the $CaAl_2Si_2O_8:Eu^{3+}$,[9] $Ca_{10}M(PO_4)_7$ (M = Li, Na, K):Eu^{2+}/Eu^{3+},[25] and $Sr_5(BO_3)_3F:Eu^{3+}$(ref. 26) samples.

Hubei Collaborative Innovation Center for Advanced Organochemical Materials, Ministry-of-Education Key Laboratory for the Synthesis and Applications of Organic Functional Molecules, Hubei University, Wuhan, Hubei, China. E-mail: liling402431@hotmail.com; liuxiaoguang402@hotmail.com

$MZn_2(PO_4)_2$ (M = Mg, Ca, Sr, Ba) is an important host with the advantages of low cost, high luminescence efficiency, low synthesis temperature and good thermal stability. Based on these characteristics, $BaZn_2(PO_4)_2$ has also become one of the hot topics of discussion. In the previous reports, the properties of $BaZn_2(PO_4)_2$ phosphors have been studied. For example, the photoluminescence properties of $BaZn_2(PO_4)_2$:Ce^{3+}, Tb^{3+}/Dy^{3+} (ref. 27 and 28) and red phosphor $BaZn_2(PO_4)_2$:Sm^{3+} (ref. 29) have been studied. However, the lattice occupancy and the self-reduction phenomenon of Eu ion doping in $BaZn_2(PO_4)_2$ and the energy transfer behavior of Ce^{3+}, Eu^{2+} co-doping in $BaZn_2(PO_4)_2$ have not been discussed.

In this work, a series of $Eu^{2+/3+}$ and Ce^{3+} single- and co-doped $BaZn_2(PO_4)_2$ products were synthesized *via* a high-temperature solid-state reaction. First, the self-reduction phenomenon was found from Eu^{3+} to Eu^{2+} in the $BaZn_2(PO_4)_2$ system. Next, we use the bond energy method to analyze the self-reduction reaction from Eu^{3+} to Eu^{2+} in the lattice position of Zn in $BaZn_2(PO_4)_2$. At the same time, we use this method to explain why Eu^{3+} can be self-reduced to Eu^{2+}. Finally, the photoluminescence properties and energy transfer mechanisms of Ce^{3+}–Eu^{2+} ion co-doped $BaZn_2(PO_4)_2$ are studied in detail. In addition, based on the energy transfer, the emission color can be adjusted from blue to white by adjusting the relative proportions of Ce and Eu ions.

2 Experimental

2.1 Preparation of phosphors

A series of $Eu^{2+/3+}$, Ce^{3+} ion single- and co-doped $BaZn_2(PO_4)_2$ phosphors were synthesized by a traditional high-temperature solid-state method in an air atmosphere. The raw materials selected include $BaCO_3$, $(NH_4)_2HPO_4$, ZnO, CeO_2 and Eu_2O_3. The exact amount of raw materials of each component was calculated, and the analytical balance was accurately and effectively weighed. The raw materials were thoroughly ground and mixed evenly in an agate mortar, and transferred to an alumina crucible of appropriate size. Then the mixtures were pre-sintered at 850 °C for 4 h, and further calcined at 1000 °C for 4 h. Finally, all the as-synthesized products were naturally cooled to room temperature and ground to a powder.

2.2 Characterization methods

The phase purity characterization of the phosphors was performed using an X-ray diffractometer. Excitation source information: 40 kV, 40 mA on a Bruker D8 Advance X-ray diffractometer with Cu Kα (λ = 1.5418 Å) radiation. The scanning mode is continuous, the scanning speed is 2° per minute, and the test range is 5–80°. The morphologies of the samples were characterized by scanning electron microscopy (SEM) on an instrument of JSM 6510 LV Electronics, Japan; the resolution is 3 nm. The spectrometer FLS980 was used to test the emission and excitation as well as decay curves of the samples. A 450 W xenon lamp was used as a steady-state light source in the test and a 60 W μF flash lamp was used as the decay curve test source.

3. Results and discussion

3.1 Phase analysis and crystal structure

Fig. 1 depicts the XRD patterns of $Eu^{2+/3+}$, Ce^{3+} ion single- and co-doped $BaZn_2(PO_4)_2$ phosphors. Compared with the standard card JCPDS#16-0554, it can be seen that the diffraction peaks of the synthesized samples corresponded well to the standard card, and no other diffraction peaks appeared. Therefore, the prepared samples were all pure phases and no impurities were formed. This indicates that rare-earth ions enter the $BaZn_2(PO_4)_2$ lattice, and no other impurity phases are formed; hence, the doping of these ions does not cause any change in the lattice structure of $BaZn_2(PO_4)_2$. However, the XRD patterns of $Eu^{2+/3+}$, Ce^{3+} ion single- and co-doped $BaZn_2(PO_4)_2$ phosphors are light-shifted compared with the pure $BaZn_2(PO_4)_2$ compound. This result could be attributed to the larger ionic radii of Eu^{3+} [r = 1.09 Å and 1.101 Å for CN = 4 and 7, respectively] and Ce^{3+} [r = 1.07 Å for CN = 7] with respect to those of Ba^{2+} (r = 1.38 Å for CN = 7, respectively) and Zn^{2+} (r = 0.60 Å for CN = 4, respectively). Moreover, as the radius of the dopant ions increase, the lattice gets distorted, and hence, the position of the diffraction peak shifts slightly.

The unit cell of $BaZn_2(PO_4)_2$ is exhibited in Fig. 2. $BaZn_2(PO_4)_2$ belongs to a monoclinic crystal structure of space group $P2_1/c$. The unit cell contains five kinds of cation coordination environments, namely Ba1, Zn1, Zn2, P1 and P2. Ba1 form isolated BaO polyhedra, which has seven coordination sites with an asymmetric polyhedron surrounded by oxygen atoms. Both Zn1 and Zn2 are tetrahedrons connected to oxygen. At the same time, there are two environments of tetrahedrons, one with vertices connected to a polyhedron centered on Ba and the other with a co-edge. P1 and P2 are also two four-coordinated sites. The parameters of the unit cell are a = 8.598 Å, b = 9.761 Å, c = 9.159 Å, and V = 768.45 Å^3, respectively.

The SEM micrograph, EDS mapping images and elemental distribution of Eu/Ce doped in $BaZn_2(PO_4)_2$ synthesized under

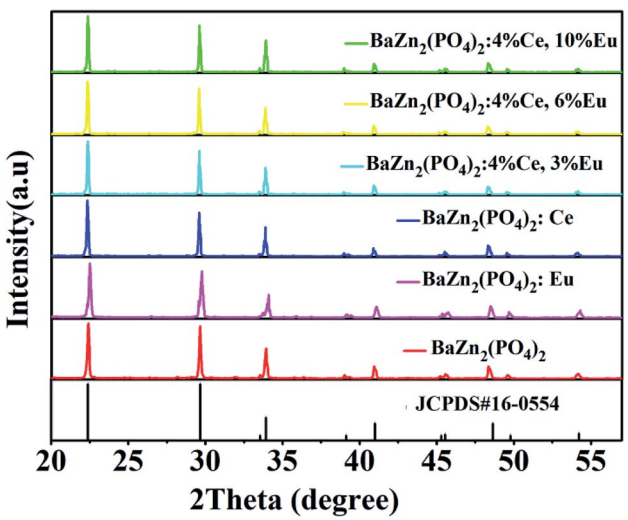

Fig. 1 XRD patterns of $Eu^{2+/3+}$, Ce^{3+} ion single- and co-doped $BaZn_2(PO_4)_2$ phosphors and standard card (JCPDS#16-0554).

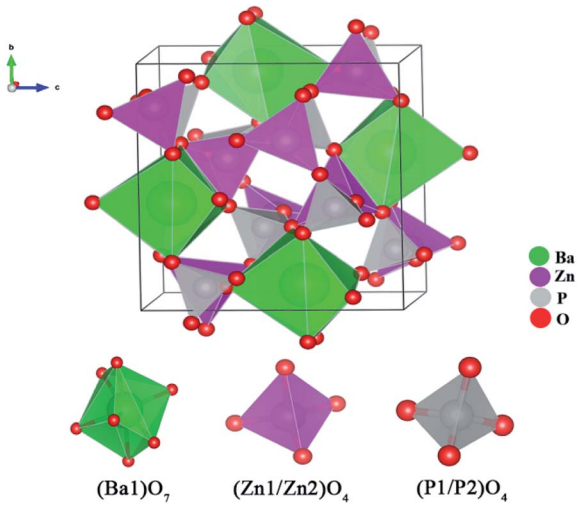

Fig. 2 Schematic of the crystal structure of $BaZn_2(PO_4)_2$ and coordination environments for Ba, Zn and P sites.

ambient conditions are displayed in Fig. 3. According to the SEM image of the two samples, we can see that all the samples have a block structure with inconsistent size. According to the EDS scanning structure and elemental distribution image, the atomic distribution patterns of Ba, O, P, Zn, Eu or Ce can be obtained very clearly in the Eu- or Ce-doped $BaZn_2(PO_4)_2$ samples. These indicate that the Ce and Eu elements are indeed present in the $BaZn_2(PO_4)_2$ sample.

3.2 Photoluminescence properties of $BaZn_2(PO_4)_2$:Eu

The excitation and emission spectra of the undoped $BaZn_2(PO_4)_2$ sample are shown in Fig. 4. At an excitation wavelength of 240 nm, the emission spectrum consists of a broad peak at a maximum wavelength position of 345 nm in the wavelength range of 300–425 nm (Fig. 4a). In the excition spectrum (Fig. 4b), the maximum wavelength position of the excitation spectrum is at 240 nm.

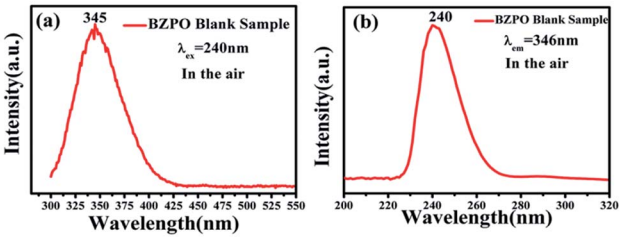

Fig. 4 (a and b) PLE ($\lambda_{ex=240\ nm}$) and PL ($\lambda_{em=345\ nm}$) spectra of the $BaZn_2(PO_4)_2$ sample.

Fig. 5 displays the photoluminescence spectra of $BaZn_2(PO_4)_2$:Eu phosphors. It can been found that a series of sharp peaks with an emission spectrum between 550–750 nm are due to the $^5D_0$–^7F_J (J = 0, 1, 2, 3, 4) transition of Eu^{3+} upon the 258 nm excitation, whose maximum wavelength position belongs to the $^5D_0$–$^7F_1$ transition at 593 nm. By monitoring the emission at 593 nm, it was found that the excitation spectrum in the range of 200–550 nm consists of a broadband excitation with a central wavelength at 258 nm, which is attributable to the charge transition of O^{2-}–Eu^{3+} and some sharp peaks can be ascribed to the characteristic excitation of Eu^{3+} in Fig. 5(a). We know that when the Eu^{3+} ion is in a position with a strict inversion center, it will be dominated by the allowable $^5D_0$–$^7F_1$ magnetic dipole transition, and the emission peak is around 590 nm. Therefore, it can be judged that in the $BaZn_2(PO_4)_2$:Eu sample we prepared, the Eu^{3+} ion occupies the inversion symmetry position. According to the asymmetrical structure centered on the Ba atom, it is presumed that the Eu^{3+} ion enters a symmetric tetrahedral structure centered on the Zn atom.

The spectrum of the phosphor $BaZn_2(PO_4)_2$:Eu at different excitation and monitoring wavelengths is shown in Fig. 5(b).

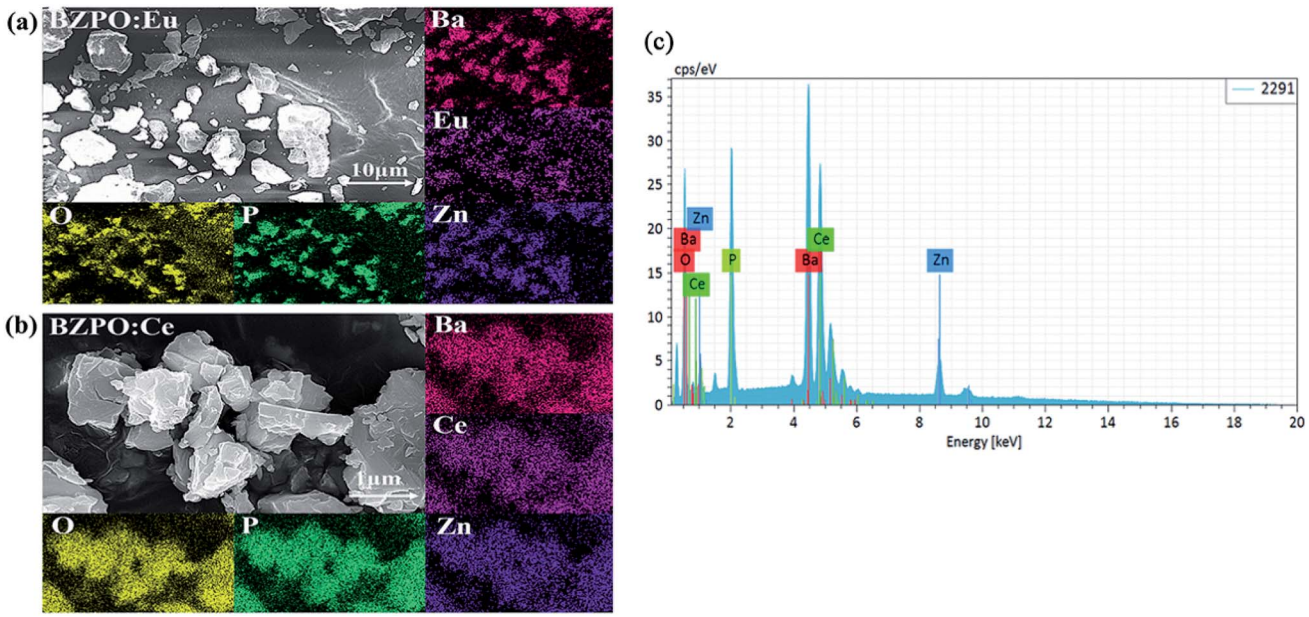

Fig. 3 (a and b) Scanning electron micrographs and EDS of $BaZn_2(PO_4)_2$:Eu/Ce. (c) Elemental distribution map of $BaZn_2(PO_4)_2$:Ce.

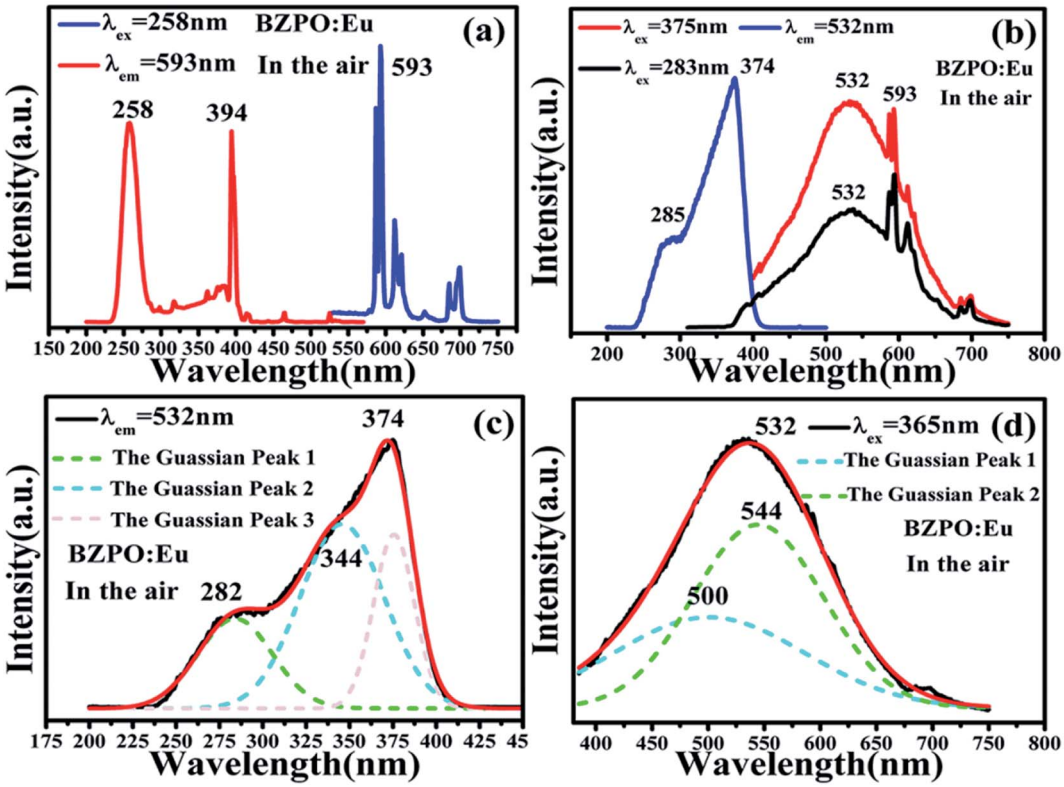

Fig. 5 (a and b) Excitation (λ_{em} = 593, 532 nm) and emission spectra (λ_{ex} = 258, 283 and 375 nm) of the $BaZn_2(PO_4)_2$:Eu sample. (c and d) Gaussian fitting excitation (λ_{em} = 532 nm) and emission band (λ_{ex} = 365 nm) of $BaZn_2(PO_4)_2$:Eu.

Upon monitoring the wavelength at 532 nm, it was found that the excitation spectrum of $BaZn_2(PO_4)_2$:Eu consists of a narrow band absorption ranging from 200 to 450 nm with the dominant absorption peak at 374 nm, which comes from the 4f → 5d transition of Eu^{2+} ions. Under the excitation of 283 and 375 nm, $BaZn_2(PO_4)_2$:Eu phosphors exhibited broad emission bands in the range of 350–750 nm with a maximum at 532 nm, which originates from the 5d → 4f transitions of Eu^{2+} ions. At the same time, the emission sharp peaks belonging to the $^5D_0$–$^7F_1$ transition of Eu^{3+} at 593 nm can also be clearly observed. Therefore, the existence of Eu^{2+} was proved. From Fig. 5(a), it can be observed that Eu^{2+} and Eu^{3+} coexist in the system, indicating that the self-reduction process from Eu^{3+} to Eu^{2+} occurred in the $BaZn_2(PO_4)_2$ crystal. We also made a Gaussian fitting to the excitation spectrum monitored at 532 nm wavelength and the emission spectrum at 365 nm wavelength, as shown in Fig. 5(c and d). The center positions of the three sub-excitation peaks obtained by Gaussian fitting are at 282, 344, and 375 nm, respectively. This is due to the splitting of the excitation peak broadband. Similarly, two sub-emission peaks of the emission spectrum are obtained with center positions at 500 and 544 nm. From this, we conclude that Eu^{2+} ions occupy two sites in the $BaZn_2(PO_4)_2$ lattice.

In $BaZn_2(PO_4)_2$ crystals, there are five kinds of cationic sites that can be occupied by the dopant, namely Ba1, Zn1, Zn2, P1 and P2. From the photoluminescence spectrum, we know that the strongest position of the emission peak of Eu^{3+} ions is at 593 nm, indicating that Eu^{3+} ions are in the inversion symmetry position and occupy the position of Zn. We use the theoretical method of bond energy to explain the reduction of Eu^{3+} to Eu^{2+} in the air and the priority of Eu^{2+} and Eu^{3+} ions in the lattice position of Zn in the system. It can be used by the following expression:

$$E_{Zn^{2+}/Eu^{3+/2+}-O^{2-}} = J \exp\left(\frac{d_0 - d_{M-O}}{0.37}\right)\left(\frac{V_N}{V_M}\right) \quad (1)$$

where V_N is the valence state of Zn^{2+} cations in the system and V_M is the number of valence states of Eu^{2+} and Eu^{3+}. For Eu^{3+} ions taken as an example, if Eu^{3+} occupies the Zn site, then $V_N/V_M = 2/3$; if the doping ion Eu^{2+} is at the Zn site, then $V_N/V_M = 1/1$. This indicates that the valence state has some effect on the bond energy of the crystal. J represents the intrinsic standard atomization energy and d_0 is equal to a constant for a given pair of atoms. The J and d_0 of the compounds involved are listed in Table 1. E_{M-O} is the bond energy value. According to formula (1), the bond energy values $E_{Zn^{2+}-O^{2-}}$, $E_{Eu^{2+}-O^{2-}}$ and $E_{Eu^{3+}-O^{2-}}$ are

Table 1 The value of J and d_0 for Zn^{2+}–O^{2-}, Eu^{3+}–O^{2-} and Eu^{2+}–O^{2-}

Ions	J (kcal mol^{-1})	d_0 (Å)
Zn^{2+}–O^{2-}	86.900	1.704
Eu^{3+}–O^{2-}	109.400	2.074
Eu^{2+}–O^{2-}	56.180	2.049

calculated and shown in Table 2. The variation of bond energy reflects the preferential occupancy of the dopant ions. Its calculation method is as follows:

$$\Delta E^{Zn^{2+}-O^{2-}}_{Eu^{2+/3+}-O^{2-}} = |E_{Zn^{2+}-O^{2-}} - E_{Eu^{2+/3+}-O^{2-}}| \quad (2)$$

where $\Delta E^{Zn^{2+}-O^{2-}}_{Eu^{2+/3+}-O^{2-}}$ is the variation in bond energy, that is, a change of bond energy caused when Eu^{2+} and Eu^{3+} ions enter the lattice to replace the Zn1 and Zn2 sites. The smaller the change in bond energy, the easier it is to be occupied by dopant ions. Here, if the bond energy change value $\Delta E^{Zn^{2+}-O^{2-}}_{Eu^{2+}-O^{2-}}$ is smaller than $\Delta E^{Zn^{2+}-O^{2-}}_{Eu^{3+}-O^{2-}}$, then the Eu^{2+} ion is more likely to occupy the position of Zn, and *vice versa*. From eqn (2), we calculated the variation in bond energy when $Eu^{2+/3+}$ ions occupy the Zn1 and Zn2 sites in the $BaZn_2(PO_4)_2$ system. The results are shown in Table 2. For $Eu^{2+/3+}$ ions, we can see that the bond energy variation values of $\Delta E^{Zn1}_{Eu^{2+}-O^{2-}}$, $\Delta E^{Zn2}_{Eu^{2+}-O^{2-}}$, $\Delta E^{Zn1}_{Eu^{3+}-O^{2-}}$ and $\Delta E^{Zn2}_{Eu^{3+}-O^{2-}}$ are 28.6619, 29.0296, 57.1607 and 57.8942, respectively. It is clear that the bond energy difference $\Delta E^{Zn}_{Eu^{2+}-O^{2-}}$ of Eu^{2+} at the Zn site is smaller than that of $\Delta E^{Zn}_{Eu^{3+}-O^{2-}}$, so Eu^{2+} is more likely to occupy this site than the Eu^{3+} ion. At the same time, this also implies that Eu^{2+} is more stable in the Zn site and it provides conditions that Eu^{3+} can be reduced to Eu^{2+} under non-reducing condition.

In summary, we calculated that when Eu^{2+} and Eu^{3+} ions are into the $BaZn_2(PO_4)_2$ matrix, the bond energy change values of Eu^{2+} and Eu^{3+} ions at the Zn1 and Zn2 sites by using the theoretical method of bond energy. The bond energy change value $\Delta E^{Zn}_{Eu^{2+}-O^{2-}}$ is smaller than $\Delta E^{Zn}_{Eu^{3+}-O^{2-}}$, indicating that Eu^{2+} is more likely to occupy the Zn site than Eu^{3+}, which also implies that Eu^{3+} can be self-reduced to Eu^{2+}. All theoretical calculations are consistent with the PL spectrum phenomenon.

Based on the principle of charge compensation mechanism,[30] when Eu^{3+} replaces the site of Zn^{2+}, the charge in the environment is unbalanced. In order to maintain the overall charge exhibiting electrical neutrality, the formation of the cationic vacancy defect V''_{Zn} will generate two negative electrons to compensate for the cation vacancy defects induced by $Eu^{\cdot}_{Zn}$. Then form a dipole complex $V^{\cdot}_{Zn}$, where $Eu^{\cdot}_{Zn}$ represents an electron donor and $Eu^{\cdot}_{Zn}$ an electron acceptor. When the negative charge generated on $V^{\cdot}_{Zn}$ is transferred to $Eu^{\cdot}_{Zn}$, Eu^{3+} will be reduced to Eu^{2+}:

$$2Eu^{3+} + 3Zn^{2+} \rightarrow V''_{Zn} + 2Eu^{\cdot}_{Zn}$$

$$V''_{Zn} \rightarrow V^{\times}_{Zn} + 2e^{-}$$

$$2Eu^{\cdot}_{Zn} + 2e^{-} \rightarrow 2Eu^{\times}_{Zn}$$

3.3 Photoluminescence properties of $BaZn_2(PO_4)_2$:Ce, Eu

Fig. 6 depicts the excitation and emission spectra of different concentrations of Ce^{3+} doped in $BaZn_2(PO_4)_2$. For Fig. 6(a), under the monitoring of 336 nm, the excitation spectrum is in the range of 230–310 nm, and the strongest absorption of these excitation bands is about 287 nm, which is due to the transition of the Ce^{3+} ion from the ground state to crystal field splitting level of the 5d state. In general, the emission spectrum of Ce^{3+} ion sample has a dual characteristic due to the ground state $^2F_{5/2}$ and $^2F_{7/2}$ spin orbital splitting, which indicates that Ce^{3+} is successfully doped into $BaZn_2(PO_4)_2$. As shown in Fig. 6(b), the emission spectra have two broad bands centered at 334 and 410 nm in the range of 300–500 nm, which can be clearly observed under the excitation at 287 nm.

The excitation spectra of the $BaZn_2(PO_4)_2$:x% Ce sample monitored at 336, 356 and 410 nm are shown in Fig. 6(c–e). We can see that the photoluminescence intensity reaches the maximum when the doping concentration of Ce^{3+} is 0.5%. At the same time, we normalized the excitation spectra under these different monitoring wavelengths, as shown in Fig. 6(f–h). At the monitoring wavelength of 336 nm, the broadband center of the excitation spectrum was located at 286 nm; it is worth noting that when the monitoring wavelength is 356 nm, the central position of the excitation spectrum changes with different concentrations of Ce^{3+} doping, that is, the central position of the broad excitation bands are 290 and 305 nm, respectively. In addition, the excitation spectrum exhibited a red shift phenomenon when monitored at 410 nm which is due to the influence of the crystal field.[31,32] By comparing the excitation spectra at different monitoring wavelengths in Fig. 6, it can

Table 2 Bond energy of Zn–O bonds in $BaZn_2(PO_4)_2$ ($E_{Zn^{2+}-O^{2-}}$) and bond energy of Eu–O bond ($E_{Eu^{2+}-O^{2-}}$, $E_{Eu^{3+}-O^{2-}}$) and variation in bond energy when $Eu^{2+/3+}$ is at the sites of Zn1 and Zn2 in $BaZn_2(PO_4)_2$ ($\Delta E^{Zn^{2+}-O^{2-}}_{Eu^{2+}-O^{2-}}$, $\Delta E^{Zn^{2+}-O^{2-}}_{Eu^{2+/3+}-O^{2-}}$). The units are kcal mol^{-1}

Central atom	Coordination atom	Count	d_{m-o}	E_{M-O}	$E_{Eu^{2+}-O^{2-}}$	$E_{Eu^{3+}-O^{2-}}$	$\Delta E^{M}_{Eu^{2+}-O^{2-}}$	$\Delta E^{M}_{Eu^{3+}-O^{2-}}$
Zn1	O2	1×	1.9168	48.8924	80.3071	111.5430	28.6619	57.1607
	O1	1×	1.9429	45.5623	74.8373	103.9458		
	O3	1×	1.959	43.6223	71.6507	99.5197		
	O6	1×	1.9878	40.3556	66.2851	92.0672		
Zn2	O7	1×	1.9065	50.2726	82.5740	114.6917	29.0296	57.8942
	O4	1×	1.9491	44.8052	73.5938	102.2185		
	O5	1x	1.9654	42.8742	70.4220	97.8131		
	O8	1x	1.9663	42.7700	70.2509	97.5755		

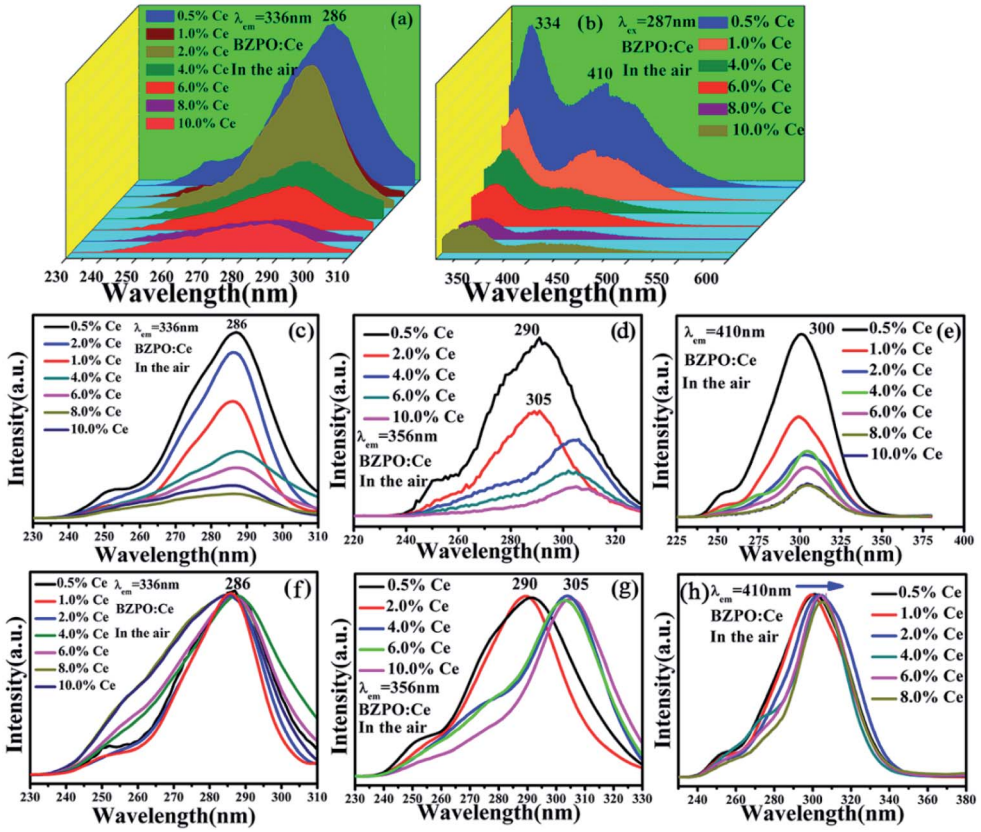

Fig. 6 (a) Excitation spectra of $BaZn_2(PO_4)_2$:x% Ce under 336 nm monitoring wavelength ($x = 0.5, 1, 2, 4, 6, 8, 10$); (b) emission ($\lambda_{ex} = 287$ nm) spectra of $BaZn_2(PO_4)_2$:x% Ce under 287 nm excitation ($x = 0.5, 1, 4, 6, 8, 10$); (c–e) the excitation spectra of $BaZn_2(PO_4)_2$:x% Ce ($x = 0.5, 1, 2, 4, 6, 8, 10$) phosphors at the monitoring wavelength of 336, 356, and 410 nm, respectively; (f–h) normalized excitation spectra monitored at 336, 356 and 410 nm, respectively.

be seen that in addition to the difference in luminescence intensity, the peak shape and the dominated peak position also have significant differences.

The emission spectrum of the $BaZn_2(PO_4)_2$:4% Ce, x% Eu series sample at an excitation wavelength of 304 nm for Ce^{3+} is shown in Fig. 7(a). There are two distinct broadband emission peaks in the range of 300–800 nm, which are the 5d–4f transitions corresponding to Ce^{3+} and Eu^{2+} at 428 and 609 nm, respectively. In the $BaZn_2(PO_4)_2$:4% Ce, x% Eu co-doped sample, not only the emission of Ce^{3+} but also the emission of Eu^{2+} was observed by the 304 nm characteristic excitation of Ce^{3+}. At the same time, it can be clearly seen that as the concentration of Eu ions increases, the luminescence intensity of Ce^{3+} ions gradually decreases, and that of Eu^{2+} ions gradually increases. This strongly proves that energy transfer occurs between Ce^{3+} and Eu^{2+}. Fig. 7(b) is the excitation spectrum obtained under the monitoring of 609 nm. It shows that there are three strong broad bands in the range of 225–550 nm, and their central positions at 248, 303 and 376 nm belong to the charge transition of O^{2-}–Eu^{3+}, the f–d energy level transition of Ce^{3+} and the 4f-5d transition of Eu^{2+}, respectively. Therefore, we found that under the monitoring of Eu^{2+}, the excitation spectrum exhibits the excitation peak of Ce^{3+}, which further proves the phenomenon of Ce^{3+}–Eu^{2+} energy transfer.

3.4 Energy transfer mechanism

In order to further study the energy transfer process, we tested the lifetime of Ce^{3+} ions under 320 nm excitation ($\lambda_{ex} = 302$ nm, $\lambda_{em} = 428$ nm) and Eu^{2+} ions under the corresponding excitation and emission wavelengths, as shown in Fig. 7(c). The decay curves are better fitted by the second-order exponential decay. The formula is as follows:[33]

$$I(t) = A_1 \exp\left(-\frac{t}{\tau_1}\right) + A_2 \exp\left(-\frac{t}{\tau_2}\right) \quad (3)$$

where $I(t)$ represents the luminescence intensity; A_1 and A_2 are the amplitude constants; t is the decay time; and τ_1 and τ_2 are the exponential components of fast and slow decay times, respectively. The average decay time (τ^*) is calculated using the following formula:

$$\tau^* = (A_1\tau_1^2 + A_2\tau_2^2)/(A_1\tau_1 + A_2\tau_2) \quad (4)$$

According to eqn (3) and (4), the decay time of Ce^{3+} in $BaZn_2(PO_4)_2$:4% Ce, x% Eu samples are approximately 1.5, 1.47, 1.42, 1.31 and 1.30 μs corresponding to $x = 3, 4, 6, 8, 10$ in Fig. 7(c). We can observe that as the concentration of Eu ions increases, the lifetime of Ce^{3+} ions decreases, whereas the lifetime of Eu^{2+} ions increases, which is in good agreement with the

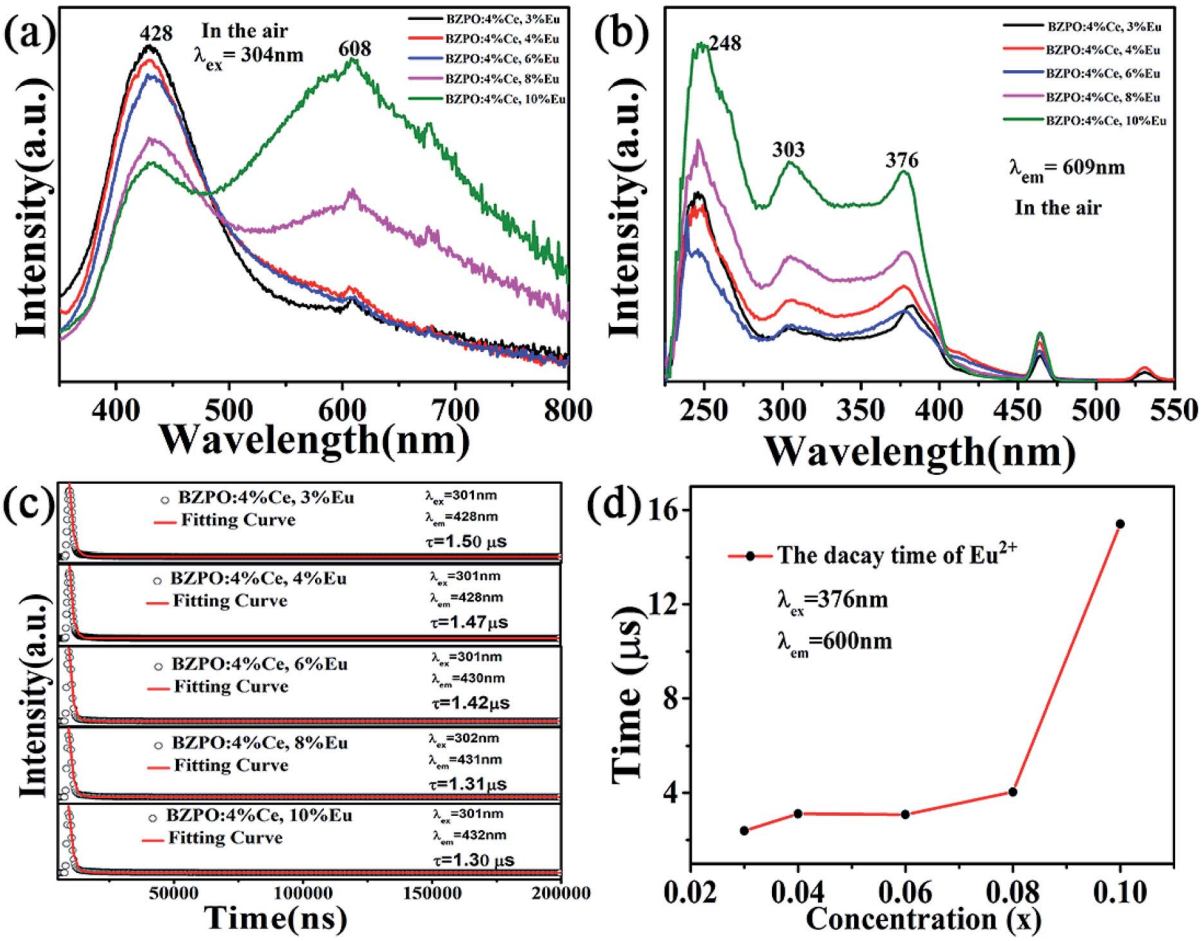

Fig. 7 (a and b) The emission spectrum of a series of $BaZn_2(PO_4)_2$:4% Ce, *x*% Eu ($x = 3, 4, 6, 8, 10$) samples excited at 304 nm and the excitation spectrum monitored at 428 nm, respectively; (c) decay lifetime of Ce^{3+} in $BaZn_2(PO_4)_2$:4% Ce, *x*% Eu; (d) variations of the decay lifetime for Eu^{2+} with the increasing Eu ion concentration in $BaZn_2(PO_4)_2$:4% Ce, *x*% Eu ($\lambda_{ex} = 376$ nm, $\lambda_{em} = 600$ nm).

spectral characteristics of $BaZn_2(PO_4)_2$:4% Ce, *x*% Eu. This also strongly indicates the energy transfer behavior between Ce^{3+} and Eu^{2+} ions.

Based on Dexter's theory, the critical distance of energy transfer is defined as the distance at which the transition probability is equal to the probability of Ce^{3+} radiation emission. The critical distance R_c for energy transfer between Ce^{3+} and Eu^{2+} in $BaZn_2(PO_4)_2$ is discussed by the following formula:[28]

$$R_c \approx 2\left[\frac{3V}{4\pi X_c N}\right]^{\frac{1}{3}} \quad (5)$$

where V represents the volume of the unit cell and X_c stands for the critical concentration of the dopant, and N is the number of available sites per unit cell. In the $BaZn_2(PO_4)_2$ crystal structure, the values of V, X_c and N are 768.45 Å^3, 0.1 and 4, respectively. The critical distance R_c is calculated to be 15.426 Å by eqn (5). We know that when the distance between two luminescence centers is less than the critical distance of 5 Å, the energy transfer between the two luminescence centers is carried out by the exchange interaction mechanism, otherwise it is through electric multipolar interactions. Therefore, it can be seen that energy transfer from Ce^{3+} to Eu^{2+} in $BaZn_2(PO_4)_2$ belongs to electrical multipole interaction. Based on Dexter's multipole interaction energy transfer formula and Reisfeld's approximation, the mechanism in the present system is applied through the following relationship:

$$\frac{I_{S0}}{I_S} \propto C^{n/3} \quad (6)$$

where I_{S0} indicates the luminescence intensity of Ce^{3+} ions when Eu^{3+} ions are not doped; I_S is equal to the luminescence intensity of Ce^{3+} ions with the presence of Eu^{2+} ions; and C stands for the sum of the concentrations when Eu^{2+} and Ce^{3+} coexist. When the value of n is 6, 8, or 10, it means dipole–dipole (d–d), dipole–quadrupole (d–q), and quadrupole–quadrupole (q–q) interactions, respectively.[34] The I_{S0}/I_S–$C^{n/3}$ plots are exhibited in Fig. 8. Obviously, when $n = 6$, 8 and 10, the linear fitting R^2 values of I_{S0}/I_S–$C^{n/3}$ are 0.9920, 0.9826 and 0.9667, respectively, that is, when $n = 6$, linear behavior is the best. Therefore, the energy transfer of Ce^{3+}–Eu^{2+} in this system follows the electric dipole–dipole interaction mechanism. The quantum efficiency was determined to be 24.58%, 29.12%,

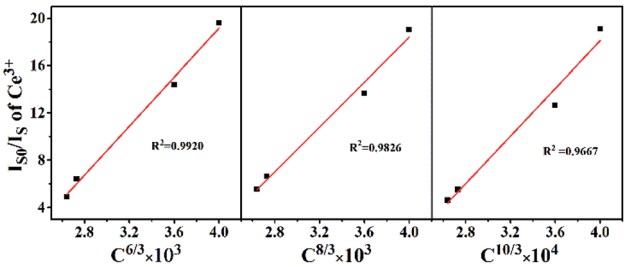

Fig. 8 Dependence of I_{S0}/I_S of Ce^{3+} on $C^{n/3}$ (n = 6, 8, 10) in the $BaZn_2(PO_4)_2$:4% Ce, x% Eu samples.

24.16%, 32.52%, and 29.02% for $BaZn_2(PO_4)_2$:4% Ce, x% Eu with x = 3, 4, 6, 8, 10, respectively.

The chromaticity calculation was performed based on the photoluminescence spectra of the $BaZn_2(PO_4)_2$:4% Ce, x% Eu phosphor at 304 nm excitation, and the calculation results of the CIE coordinates are shown in Fig. 9. Detailed CIE chromaticity coordinates are listed in Table 3. In a series of samples of $BaZn_2(PO_4)_2$:4% Ce, x% Eu, as the doping concentration of Eu ions is from 0.03 to 0.1, we can see that the CIE coordinates of the samples change from the blue region to the white region. It is worth noting that the CIE chromaticity coordinates of the $BaZn_2(PO_4)_2$:4% Ce, 8% Eu sample in the white light region (0.3195, 0.2959) is very close to the ideal white luminescence chromaticity coordinates (0.33, 0.33). It is suggested that the $BaZn_2(PO_4)_2$:4% Ce, 8% Eu phosphor has suitable color coordinates as white phosphors in the field of lighting. The results show that the light emission of white phosphors can be achieved by appropriately adjusting the ratio of Ce/Eu ions.

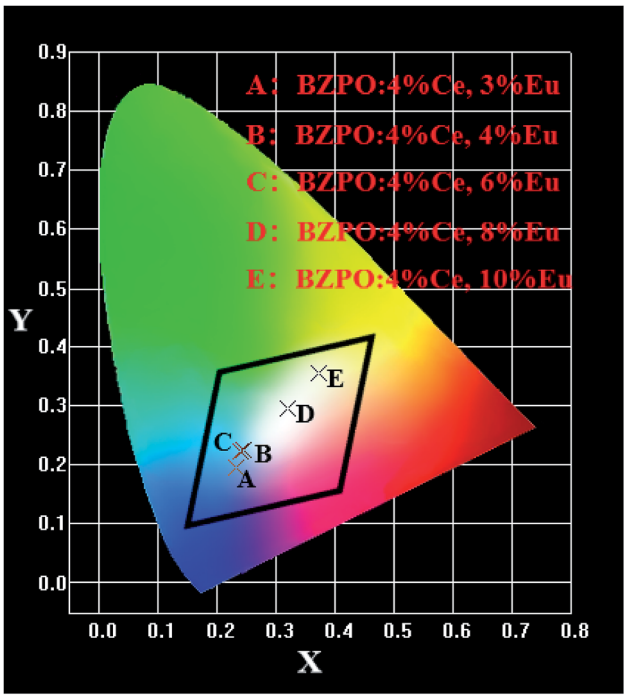

Fig. 9 CIE chromaticity diagram for $BaZn_2(PO_4)_2$:4% Ce, x% Eu under 304 nm excitation (x = 3, 4, 6, 8, 10).

Table 3 CIE chromaticity coordinates of $BaZn_2(PO_4)_2$:4% Ce, x% Eu (x = 3, 4, 6, 8, 10)

Point	Sample	CIE (x, y)	Peak	Peak intensity
A	BZPO:4% Ce, 3% Eu	(0.2318, 0.1939)	430	1256820
B	BZPO:4% Ce, 4% Eu	(0.2450, 0.2238)	429	1201980
C	BZPO:4% Ce, 6% Eu	(0.2404, 0.2226)	428	1146960
D	BZPO:4% Ce, 8% Eu	(0.3195, 0.2959)	429	910659
E	BZPO:4% Ce, 10% Eu	(0.3718, 0.3562)	608	1208720

4. Conclusions

A series of novel $Eu^{2+/3+}$, Ce^{3+} ion single- and co-doped $BaZn_2(PO_4)_2$ samples have been synthesized *via* a high-temperature solid-state reaction. It was confirmed by XRD powder diffraction that our target products are all pure phases. The self-reduction from Eu^{3+} to Eu^{2+} has been found in the $BaZn_2(PO_4)_2$ system. The photoluminescence spectra show that Eu^{2+} and Eu^{3+} ions coexist in the $BaZn_2(PO_4)$ crystal. At the same time, the strongest emission peak of Eu^{3+} ions belongs to the $^5D_0$–$^7F_1$ transition of Eu^{3+} at 593 nm, which indicates that Eu^{3+} ions occupy the inversion symmetry lattice and occupy the site of Zn in $BaZn_2(PO_4)$. According to the bond energy method, the priority of Eu^{2+} and Eu^{3+} ions in the lattice position of Zn and the self-reduction of Eu^{3+} to Eu^{2+} were explained in $BaZn_2(PO_4)$. The results indicate that the value $\Delta E^{Zn}_{Eu^{2+}-O^{2-}}$ is smaller than $\Delta E^{Zn}_{Eu^{3+}-O^{2-}}$, indicating that Eu^{2+} is more likely to occupy the Zn site and is more stable than Eu^{3+} in $BaZn_2(PO_4)$, which also explains why Eu^{3+} ion can reduce to Eu^{2+} ion. For $BaZn_2(PO_4)_2$:4% Ce, x% Eu phosphors, the energy transfer from Ce^{3+} to Eu^{2+} was deduced by excitation and emission spectra, which was further confirmed by the decrease in the decay lifetime of Ce^{3+} as the concentration of Eu ions gradually increases. The energy transfer mechanism between Ce^{3+} and Eu^{2+} proved to be a dipole–dipole interaction. Moreover, the CIE chromaticity coordinates show that the emission color of $BaZn_2(PO_4)_2$:4% Ce, x% Eu phosphors can be changed from blue to white. In particular, the chromaticity coordinates (0.3195, 0.2959) of $BaZn_2(PO_4)_2$:4% Ce, 8% Eu are very close to the ideal white luminescence (0.33, 0.33), indicating that the phosphor has potential applications in white LEDs.

Conflicts of interest

There are no conflicts to declare.

Acknowledgements

This work is financially supported by the National Natural Science Foundations of China (Grant no. 21301053) and Hubei Natural Science Foundations from Science and Technology Department of Hubei Province (2018CFB517), Ministry-of-Education Key Laboratory for the Synthesis and Applications of Organic Functional Molecules (KLSAOFM1804).

Notes and references

1 K. Biswas, S. Balaji, D. Ghosh, A. D. Sontakke and K. Annapurna, *J. Alloys Compd.*, 2014, **608**, 266–271.
2 X. Zhang, L. Huang, F. Pan, M. Wu, J. Wang, Y. Chen and Q. Su, *ACS Appl. Mater. Interfaces*, 2014, **6**, 2709–2717.
3 X. Zhang, J. Wang, L. Huang, F. Pan, Y. Chen, B. Lei, M. Peng and M. Wu, *ACS Appl. Mater. Interfaces*, 2015, **7**, 10044–10054.
4 X. Zhang, J. Yu, J. Wang, C. Zhu, J. Zhang, R. Zou, M. Wu, B. Lei and Y. Liu, *ACS Appl. Mater. Interfaces*, 2015, **7**, 28122–28127.
5 S. K. Jaganathan, A. J. Peter, V. Mahalingam and R. Krishnan, *J. Mater. Sci.: Mater. Electron.*, 2019, **30**, 2037–2044.
6 K. H. Jang, N. M. Khaidukov, V. P. Tuyen, S. I. Kim, Y. M. Yu and H. J. Seo, *J. Alloys Compd.*, 2012, **536**, 47–51.
7 M. Keskar, S. K. Gupta, R. Phatak, S. Kannan and V. Natarajan, *J. Photochem. Photobiol., A*, 2015, **311**, 59–67.
8 M. Xia, Z. Ju, H. Yang, Z. Wang, X. Gao, F. Pan and W. Liu, *J. Alloys Compd.*, 2018, **739**, 439–446.
9 L. Li, Y. Pan, W. Wang, Y. Zhu, W. Zhang, H. Xu, L. Zhou and X. Liu, *J. Alloys Compd.*, 2018, **731**, 496–503.
10 M. V. d. S. Rezende, M. E. G. Valerio and R. A. Jackson, *Mater. Res. Bull.*, 2015, **61**, 348–351.
11 Y. Pan, W. Wang, Y. Zhu, H. Xu, L. Zhou, H. M. Noh, J. H. Jeong, X. Liu and L. Li, *RSC Adv.*, 2018, **8**, 23981–23989.
12 Y. Chu, Z. Liu, Q. Zhang, H. Fang, Y. Li and H. Wang, *J. Alloys Compd.*, 2017, **728**, 307–313.
13 H. Li and Y. Wang, *Inorg. Chem.*, 2017, **56**, 10396–10403.
14 T. Li, P. Li, Z. Wang, S. Xu, Q. Bai and Z. Yang, *Phys. Chem. Chem. Phys.*, 2017, **19**, 4131–4138.
15 W. Chen, X. Chen, F. Sun and X. Wang, *J. Alloys Compd.*, 2017, **698**, 565–570.
16 H. J. Lee, S. H. Choi, K. P. Kim, H. H. Shin and J. S. Yoo, *Jpn. J. Appl. Phys.*, 2010, **49**, 102101.
17 C. Cao, H. K. Yang, J. W. Chung, B. K. Moon, B. C. Choi, J. H. Jeong and K. H. Kim, *J. Mater. Chem.*, 2011, **21**, 10342–10347.
18 F. Huang, J. Cheng, X. Liu, L. Hu and D. Chen, *Opt. Express*, 2014, **22**, 20924–20935.
19 L. Zhang, Z. Fu, Z. Wu, Y. Wang, X. Fu and T. Cui, *Mater. Res. Bull.*, 2014, **56**, 65–70.
20 M. Shang, S. Liang, H. Lian and J. Lin, *Inorg. Chem.*, 2017, **56**, 6131–6140.
21 J. Li, L. Chen, Z. Hao, X. Zhang, L. Zhang, Y. Luo and J. Zhang, *Inorg. Chem.*, 2015, **54**, 4806–4810.
22 R. Shi, G. Liu, H. Liang, Y. Huang, Y. Tao and J. Zhang, *Inorg. Chem.*, 2016, **55**, 7777–7786.
23 R. Shi, Y. Huang, Y. Tao, P. Dorenbos, H. Ni and H. Liang, *Inorg. Chem.*, 2018, **57**, 8414–8421.
24 X. Kang, W. Lu, H. Wang and D. Ling, *Mater. Res. Bull.*, 2018, **108**, 46–50.
25 W. Wang, Y. Pan, Y. Zhu, H. Xu, L. Zhou, H. M. Noh, J. H. Jeong, X. Liu and L. Li, *Dalton Trans.*, 2018, **47**, 6507–6518.
26 Y. Zhu, Y. Pan, W. Wang, Z. Xu, Q. Luo, L. Zhou, X. Liu and L. Li, *Ceram. Int.*, 2019, **45**, 14360–14365.
27 Y. Huang, K. Jang, H. S. Lee, E. Cho, J. Jeong, S.-S. Yi, J. H. Jeong and J. H. Park, *Phys. Procedia*, 2009, **2**, 207–210.
28 L. Wang, M. Xu, H. Zhao and D. Jia, *New J. Chem.*, 2016, **40**, 3086–3093.
29 Z. Wang, P. Li, Z. Yang and Q. Guo, *J. Lumin.*, 2012, **132**, 1944–1948.
30 G. Zhu, Y. Shi, M. Mikami, Y. Shimomura and Y. Wang, *Mater. Res. Bull.*, 2014, **50**, 405–408.
31 P. Dorenbos, *Phys. Rev. B: Condens. Matter Mater. Phys.*, 2000, **62**, 15640–15649.
32 P. Dorenbos, *J. Lumin.*, 2000, **91**, 155–176.
33 M. Jiao, N. Guo, W. Lu, Y. Jia, W. Lv, Q. Zhao, B. Shao and H. You, *Inorg. Chem.*, 2013, **52**, 10340–10346.
34 G. Li, D. Geng, M. Shang, Y. Zhang, C. Peng, Z. Cheng and J. Lin, *J. Phys. Chem. C*, 2011, **115**, 21882–21892.